

Searching for the QCD critical end point using multipoint Padé approximations

D. A. Clarke¹, P. Dimopoulos², F. Di Renzo², J. Goswami³, C. Schmidt⁴, S. Singh⁴, and K. Zambello⁵

¹*Department of Physics and Astronomy, University of Utah, Salt Lake City, Utah, USA*

²*Dipartimento di Scienze Matematiche, Fisiche e Informatiche, Università di Parma and INFN, Gruppo Collegato di Parma, I-43100 Parma, Italy*

³*RIKEN Center for Computational Science, Kobe 650-0047, Japan*

⁴*Universität Bielefeld, Fakultät für Physik, D-33615 Bielefeld, Germany*

⁵*Dipartimento di Fisica dell'Università di Pisa and INFN-Sezione di Pisa, Largo Pontecorvo 3, I-56127 Pisa, Italy*



(Received 2 June 2024; accepted 14 October 2025; published 24 November 2025)

Using the multipoint Padé approach, we locate Lee-Yang edge singularities of the quantum chromodynamics (QCD) pressure in the complex baryon chemical potential plane. These singularities are extracted from singularities in the net baryon-number density calculated in $N_f = 2 + 1$ lattice QCD at physical quark mass and purely imaginary chemical potential. Taking an appropriate scaling ansatz in the vicinity of the conjectured QCD critical end point, we extrapolate the singularities on $N_\tau = 6$ lattices to pure real baryon chemical potential to estimate the position of the critical end point (CEP). We find $T^{\text{CEP}} = 102^{+11}_{-23}$ MeV and $\mu_B^{\text{CEP}} = 428^{+162}_{-74}$ MeV, which compares well with recent estimates in the literature. For the slope of the transition line at the critical point we find $-0.16(20)$.

DOI: [10.1103/y6kg-ry8x](https://doi.org/10.1103/y6kg-ry8x)

Introduction. A central goal of the experimental program at the Relativistic Heavy-Ion Collider (RHIC) of Brookhaven National Laboratory (BNL) in the U.S. and at the Large Hadron Collider (LHC) at CERN, Switzerland is the exploration of the phase diagram of quarks and gluons in the plane of temperature T and baryon chemical potential μ_B as described by the theory of the strong interaction, quantum chromodynamics (QCD). At low T and μ_B , QCD matter is known to exist as a gas of hadrons. At high T and/or μ_B , hadrons start to melt and quark-gluon plasma (QGP) is created. The QGP created at high μ_B may experience a sharp first-order phase transition as it cools, with bubbles of QGP and hadrons coexisting at a well-defined temperature. The coexistence region ends in a critical point (CEP), where QGP and hadronic matter become indistinguishable. The conjectured CEP belongs to the 3D, $Z(2)$ universality class.

Progress in understanding the phase diagram at $\mu_B > 0$ from first-principle lattice QCD calculations, in particular locating the CEP, is impeded by the infamous sign problem. In spite of this difficulty, lattice calculations are able to provide some controlled information of the phase diagram

at sufficiently small μ_B/T . This is accomplished using various techniques, for instance reweighting [1,2], analytic continuation from purely imaginary μ_B [3,4], and Taylor expansion in μ_B/T [5,6]. The Taylor expansion technique, while highly successful, is severely limited by the computational power required to compute higher-order Taylor coefficients, with state-of-the-art calculations achieving eighth order [7,8]. In response to this challenge, various resummation schemes have been proposed [9–11], which all attempt to probe deeper into the phase diagram without having to compute even higher-order cumulants. Recently the STAR collaboration has found tantalizing evidence of the hint of a QCD critical point [12,13] in the net proton fluctuation data. However, from the analysis of the QCD equation of state [14,15] using Taylor expansion and Padé approximation, it is concluded that the CEP is likely not located in the energy range of the beam energy scan II (BESII) program at RHIC in collider mode.

In this paper we adopt the multipoint-Padé resummation method introduced in [16]. The method uses information from simulations at purely imaginary μ_B to construct a Padé approximation to the logarithm of the QCD grand partition function $\log Z_{\text{QCD}}$ for complex μ_B . We then determine singularities of the approximant to estimate the CEP location. In particular we consider temperaturelike and magnetizationlike couplings t and h near the CEP. Then according to the Lee-Yang theorem [17] applied to the universal theory, 3D $Z(2)$, at $t = 0$, zeroes of Z_{QCD} in the

Published by the American Physical Society under the terms of the [Creative Commons Attribution 4.0 International license](https://creativecommons.org/licenses/by/4.0/). Further distribution of this work must maintain attribution to the author(s) and the published article's title, journal citation, and DOI. Funded by SCOAP³.

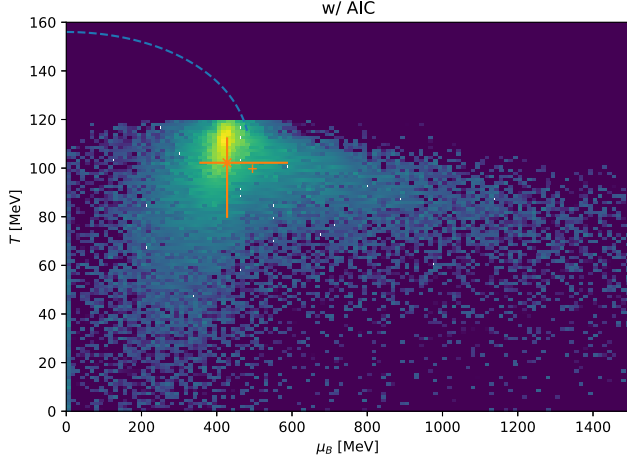


FIG. 1. Probability distribution of the QCD critical point from extrapolating Lee-Yang singularities to the real domain using universal scaling. For a detailed description see the text.

complex h -plane that approach the real axis in the thermodynamic limit correspond to phase transitions. For $t > 0$, the closest singularities to the origin are the Lee-Yang edges (LYE). We extrapolate the position of the singularity to the CEP by following LYE scaling [18].

From model calculations and model-independent symmetry arguments we understand that the location of T^{CEP} has to be searched below the chiral transition temperature $T_c^{\text{chiral}} \approx 132$ MeV [19]. Thus, we extend our calculations down to $T = 120$ MeV in this paper. Our final results are summarized in Fig. 1. We note that they are consistent with the bounds on T and μ_B mentioned above.

Lattice simulation details. We generated configurations for a $N_\sigma^3 \times N_\tau = 36^3 \times 6$ lattice and $N_f = 2 + 1$ dynamical highly improved staggered quarks (HISQ) [20] using the SIMULATEQCD [21,22] implementation of the rational hybrid Monte Carlo algorithm (RHMC) [23]. We choose bare parameters along the line of constant physical pion mass obtained for the ratio of light to strange quark mass $m_s/m_l = 27$ in Refs. [24–26]. The simulations run at 10 pure imaginary μ_B in the range $\mu_B/T \in [0, i\pi]$ to avoid the sign problem. For simplicity we set light and strange quark chemical potentials to equal values, $\mu_l = \mu_s$, which corresponds to baryon chemical potential $\mu_B = 3\mu_l$ and zero strangeness chemical potential $\mu_S = 0$. A number of configurations ranging from 1800 to 24000 was generated for a set of five temperatures ($T = 166.6, 157.5, 145.0, 136.1$ and 120.0 MeV) extending far below the chiral transition temperature as summarized in Table I. The configurations are separated by 10 molecular dynamic time units (MDTU).

We measured the first- and second-order cumulants of the net baryon-number density, defined as

$$\chi_n^B = \frac{N_\tau^3}{N_\sigma^3} \left(\frac{\partial}{\partial \hat{\mu}_B} \right)^n \log Z_{\text{QCD}}. \quad (1)$$

TABLE I. Summary of statistics for each ensemble used in this study. The last column gives approximate number of thermalized configurations per μ value. Quark masses are fixed to their physical value and $\mu_s = \mu_l$.

| β | T [MeV] | N_μ | N_{conf}/N_μ |
|---------|-----------|---------|-------------------------|
| 6.170 | 166.6 | 10 | 1800 |
| 6.120 | 157.5 | 10 | 4780 |
| 6.038 | 145.0 | 10 | 5300 |
| 5.980 | 136.1 | 10 | 6840 |
| 5.850 | 120.0 | 10 | 24000 |

A total of 500 random vectors were used to construct unbiased noisy estimators of the observables. Numerical results are illustrated in Fig. 2. The first-order cumulant is a pure imaginary, odd, and 2π -periodic function of μ_B/T whose signal gets damped as the temperature is decreased. Conversely the second-order cumulant is a pure real, even, and 2π -periodic function of μ_B/T .

Mapping poles of the multipoint Padé to Lee-Yang edge singularities. The first-order cumulant is approximated by a rational function of the form

$$R_N^N(\hat{\mu}_B) = \frac{\sum_{i=0}^N a_i \hat{\mu}_B^i}{1 + \sum_{j=1}^N b_j \hat{\mu}_B^j}, \quad (2)$$

with $N = 3, 4$ and 5 . As discussed in our original work [16], we use a rational approximation for its ability to capture or mimic singularities through poles in the denominator. Asking the coefficients a_i and b_i to reproduce the Taylor series for the first-order cumulant for multiple pure imaginary $\hat{\mu}_B$ defines our multipoint Padé. In the generalized least square process [16], data of the first two cumulants are taken into account. The fit interval $[\hat{\mu}_{\text{min}}, \hat{\mu}_{\text{max}}]$ is contained in $[-i\pi, +i\pi]$, and the length $\hat{\mu}_{\text{max}} - \hat{\mu}_{\text{min}}$ is varied between π and 2π . In this way we construct 55 rational approximations with fixed order per temperature. We obtain the poles of the rational approximation by calculating the roots of the polynomial in the denominator. The next step in the analysis requires filtering out *spurious poles*. Based on our previous experience with constructing the multipoint Padé ansatz from noisy Taylor coefficients [16,27], these spurious poles usually come in three forms: (a) residue zero poles coming from cancellations of denominator roots versus numerator roots, (b) unstable poles with respect to Padé order, and (c) poles that appear far outside the interpolated interval.¹ These properties have been clearly confirmed to hold true in our

¹A nontrivial rational function (i.e., one which is not just a polynomial) always has uncanceled poles: in the limiting case of an analytic function, these are found far away from the region one probes; on the other side, if more than one pole are found not far away, one should trust the closest to the center of the fit interval.

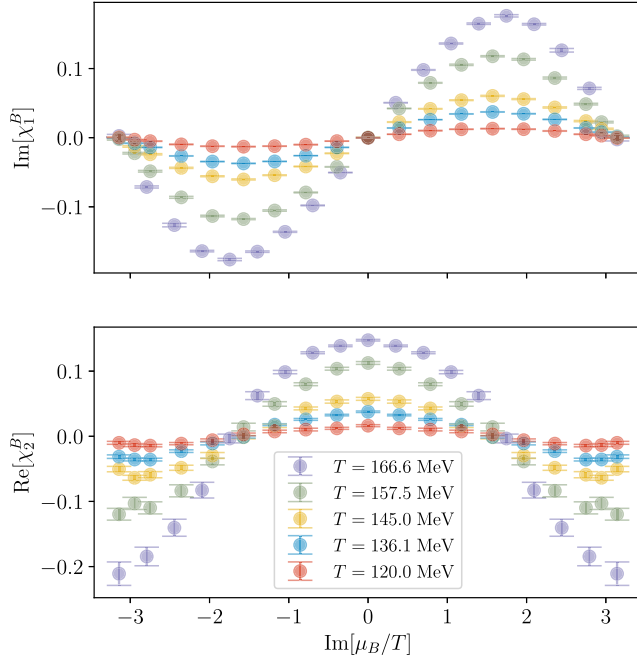


FIG. 2. First (top) and second (bottom) order net baryon-number cumulants at $T = 166.6, 157.5, 145.0, 136.1$ and 120.0 MeV. The points in the interval $[0, i\pi]$ are calculated, the points in $[-i\pi, 0]$ are obtained by reflection symmetry.

previous experience with the method, not only in [16], but also in the well-known arena of the 2D Ising model [27], thus enhancing our confidence in the numerical approach. Apart from this, one typically gets four copies of the roots coming from complex conjugation and $\mu \rightarrow -\mu$ symmetry of the partition function at finite μ_B . Further studies that discuss the treatment of spurious poles from the single point Padé ansatz in the context of the QCD critical end point are Ref. [28–30]. Hence, after doing the filtration process described above, we keep only the roots in the first quadrant and pick the one which is closest to the center of our fit interval. For each fit interval and temperature we repeat the calculation of poles on $\mathcal{O}(200)$ samples, generated by bootstrapping over the standard deviation of the cumulant data. In this way we generate distributions of poles which we represent as 1σ -confidence ellipses, as shown in Fig. 3 for a particular choice of intervals. The solid ellipses indicate results from the [3, 3]-Padé, while transparent ellipses stem from results of the [5, 5]-Padé. The difference indicates the systematic error associated with the order of the Padé. We observe that the imaginary part of the poles decreases with decreasing temperature. The solid gray line in Fig. 3 stems from a scaling fit as described below. We note that for $T > 170$ MeV, the poles accumulate on the dashed line in Fig. 3 and follow a scaling associated with the Roberge-Weiss transition in QCD [16,31,32].

Estimation of CEP location. The QCD CEP is expected to belong to the 3D, $Z(2)$ universality class. The mapping

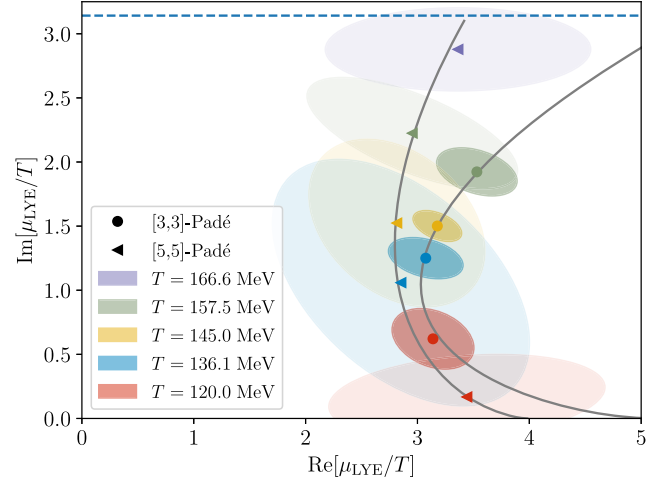


FIG. 3. Singularities from [3, 3]- and [5, 5]-multipoint Padé at temperatures $T = 166.6, 157.5, 145.0, 136.1,$ and 120.0 MeV. The dashed line indicates $\hat{\mu}_B = i\pi$.

from the control parameters T and μ_B to the temperaturelike and magnetizationlike scaling directions t and h of the Ising model is not known. We thus adopt a frequently used linear ansatz for the mapping [33–36],

$$\begin{aligned} t &= A_t \Delta T + B_t \Delta \mu_B, \\ h &= A_h \Delta T + B_h \Delta \mu_B, \end{aligned} \quad (3)$$

with $\Delta T \equiv T - T^{\text{CEP}}$, $\Delta \mu_B \equiv \mu_B - \mu_B^{\text{CEP}}$, and mixing parameters A_i, B_i . From the perspective of the renormalization group, this mapping should be valid sufficiently close to the CEP. Further away from the CEP, higher-order terms may become important.

For the extrapolation of the poles to the real axis, we would like to follow the path of the LYE. Expressed in terms of the scaling variable $z \equiv t/|h|^{1/\beta\delta}$, it has a constant position [18]

$$z_{\text{LYE}} = |z_{\text{LYE}}| e^{i\pi/2\beta\delta}. \quad (4)$$

Here β, δ are the well known critical exponents of the 3D, $Z(2)$ universality class; we use the values $\beta = 0.326419$, $\delta = 4.78984$ [37]. For a discussion of the universal constant $|z_{\text{LYE}}|$ see [38–41]. Plugging Eq. (3) into Eq. (4) then implies that μ_{LYE} should scale [42] as

$$\begin{aligned} \text{Re } \mu_{\text{LYE}} &= \mu_B^{\text{CEP}} + c_1 \Delta T + c_2 \Delta T^2 + \mathcal{O}(\Delta T^3) \\ \text{Im } \mu_{\text{LYE}} &= c_3 \Delta T^{\beta\delta}, \end{aligned} \quad (5)$$

where the coefficients c_i are functions of A_i, B_i . In particular we have $c_1 = A_h/B_h$, which denotes the slope of the transition line at the CEP in the (T, μ_B) -diagram. Note that the presence of the coefficient c_2 goes beyond the linear ansatz of Eq. (3) but seems important to extrapolate

our current data, in other words, our temperature range is wide enough to include contributions beyond the linear region. *A posteriori*, our analysis shows that the ΔT^2 contribution to the change in $\text{Re } \mu_{\text{LYE}}$ is roughly 20% for our smallest temperature.

We use Eq. (5) to simultaneously fit the real and imaginary parts of our singularities. In total the fit has 5 parameters, μ_B^{CEP} , T^{CEP} , c_1 , c_2 , and c_3 . We checked that separate fits to real and imaginary parts give very similar results with slightly reduced errors.

Results for the CEP. We perform $\mathcal{O}(10^5)$ different fits by varying the rational approximation for each temperature, based on different orders (N), intervals and bootstrapping over the numerical error of the data. The results for the coordinates of the CEP are presented in Fig. 1 as a histogram, weighted with the Akaike information criterion (AIC). The median and the 68% confidence interval is estimated and presented in Fig. 1 by star symbols and error bars. In addition we show the arithmetic mean, represented by a plus symbol. The results are in good agreement with each other, however, for the final result we pick the AIC-weighted median and find

$$(T^{\text{CEP}}, \mu_B^{\text{CEP}}) = (102_{-23}^{+11}, 428_{-74}^{+162}) \text{ MeV}, \quad (6)$$

where the errors cover statistical and systematic effects. When comparing with results from fits where bootstrapping over the statistical error was omitted, we find that both statistical and systematic errors are of similar size (see Supplemental Material [43]). Also plotted in Fig. 1 as a blue, dashed line is the crossover temperature. It is interesting to note that the histograms indicate two branches in the tails of the distribution. Whether these branches contain further information on the QCD phase diagram, e.g., on binodal or spinodal lines, will be interesting to investigate in future publications.

In order to compare the $N_\tau = 6$ results from imaginary chemical potential calculations with the eighth-order Taylor expansion results from $N_\tau = 8$ [7], the fit with the smallest $\chi^2/\text{d.o.f.}$ is presented in Fig. 4. The same fit is applied to the singularities extracted from the [4,4]-Padé resummation of the pressure expansion presented in [7]. Note that for the multipoint Padé results the rational approximation for each temperature is different, including the order of the approximation. The blue and green ellipses drawn in Fig. 4 are the 68%-confidence ellipses obtained from the covariance matrix of the fit parameters. The orange square gives the estimate of the AIC-weighted median over all $N_\tau = 6$ fits. The error bands on the fit are obtained with error propagation implemented in the AnalysisToolbox [44], which is also used to carry out the fits. From the Fig. 4 data points and fits of $N_\tau = 6$ and $N_\tau = 8$ calculations are compatible within large errors; the $\text{Im } \mu \rightarrow 0$ extrapolated location of

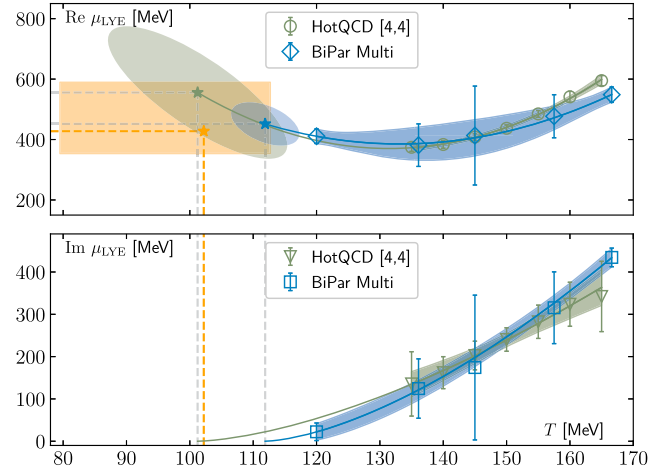


FIG. 4. Scaling fits for the LYE singularities related to the CEP. Green data come from a [4, 4] Padé from Ref. [7]. Blue data come from the multipoint Padé. Top: scaling of the real part. Bottom: scaling of the imaginary part. The ellipses shown in the top panel represent the 68% confidence region deduced from the covariance matrix of the fit. The orange box indicates the AIC weighted estimate (6).

the CEP might, however, indicate some cutoff effects. The fit parameters are summarized in Table II.

Systematic errors. The analysis is subject to several systematic uncertainties, some of which we account for and others which will be further investigated in future work. This includes (i) finite volume effects, (ii) effects related to the rational approximation and (iii) effects of the finite lattice cutoff. Regarding (i), we note that our physical volumes have the size $N_\sigma/N_\tau = 6$ and are thus larger than most of the finite temperature lattice simulations at physical quark masses. We can also estimate the finite volume effects from [45], from which we conclude that simulations with $N_f = 2 + 1$ HISQ fermions are very close to the infinite volume limit, for chiral and deconfinement observables, below a temperature of 170 MeV. In addition to the finite size effects of the data, one might discuss a correction to the infinite size scaling ansatz (5) which we investigated in [16]. The constant correction to the imaginary part turned out to be small and would shift T^{CEP} toward larger values. We estimate that such a correction would be at most 10–20 MeV ($\hat{\mu}_B \lesssim 0.1$). Preliminary results on the finite size scaling of the LYE have been presented in [46]. The effects (ii) stem from two sources: the fit range chosen for the rational approximation and the order of the approximation. The influence of the range has been assessed in this work through a sliding window analysis. We find the systematic uncertainty to be of similar magnitude as the statistical errors. The effect of the order has been investigated by varying the rational approximation between the order $N = 3$ and $N = 5$. The investigation of (iii) is beyond the scope of this study and needs calculations on lattices with

TABLE II. Obtained fit parameters from the fit with Eq. (5) to the real and imaginary parts of the singularities of $\log Z$. For $N_\tau = 6$, we show the results for the “best fit” with the smallest $\chi^2/\text{d.o.f.}$ (0.043), as well as the median and 1σ -percentiles of all performed fits, weighted with and without the Akaike information criterion (AIC).

| | $N_\tau = 6$ multipoint Padé | | | $N_\tau = 8$ [4,4]-Padé | | |
|----------|------------------------------|----------------------------|----------------------|-------------------------|----------------------------|-----------------|
| | T^{CEP} [MeV] | μ_B^{CEP} [MeV] | μ_B/T | T^{CEP} [MeV] | μ_B^{CEP} [MeV] | μ_B/T |
| best fit | 111.9 ± 5.4 | 451.7 ± 72 | 4.04 ± 0.37 | 101 ± 15 | 560 ± 140 | 5.5 ± 1.7 |
| w/AIC | $102.2 + 10.5 - 22.7$ | $427.5 + 161.9 - 73.9$ | $4.14 + 2.65 - 0.58$ | | | |
| w/o AIC | $101.7 + 10.9 - 24.1$ | $424.2 + 147.9 - 77.3$ | $4.11 + 2.58 - 0.59$ | | | |
| | c_1 | c_2 | c_3 | c_1 | c_2 | c_3 |
| best fit | -6.2 ± 7.6 | 0.15 ± 0.12 | 0.83 ± 0.14 | -12.3 ± 8.1 | 0.203 ± 0.059 | 0.55 ± 0.25 |

$N_\tau > 6$. The difference in central values between $N_\tau = 6$ and $N_\tau = 8$ data may point to cutoff effects, though these are difficult to estimate as the $N_\tau = 8$ data come from a single-point Padé of data from $\mu_B = 0$ simulations. In particular, the blue and green ellipses in Fig. 4, while possibly hinting at non-negligible cutoff dependence, are still compatible within large uncertainties. In addition, the work done in [30] compares $N_\tau = 12$ data from WB with $N_\tau = 8$ data from HotQCD and finds compatible locations for T^{CEP} . Altogether this can be taken as evidence that the cutoff effects are at worst commensurate with our current uncertainties.

Slope of the transition line. Besides the location of the CEP, we can also estimate the slope of the transition line at the CEP. In the μ_B, T -diagram, the slope is given as $1/c_1 = -0.16(20)$. Since the direction of the temperature-like scaling field t is tangential to the transition line at the CEP, we can also estimate the angles between the t -axis and the axes of the μ_B, T -diagram

$$\angle(t, T) = 81^\circ \pm 11^\circ \quad \angle(t, \mu_B) = 9^\circ \pm 11^\circ. \quad (7)$$

We note that the map in Eq. (3) can be decomposed into translations, rotations and scales [47]. In this case one of the above angles directly enters the mapping between the QCD parameter and the scaling fields.

Discussion. An important consistency check for our results on the CEP location is the comparison with the crossover line. A natural parametrization of the pseudocritical temperature T_{pc} is given as

$$T_{pc}(\mu_B) = T_{pc,0}(1 - \kappa_2 f^2(\mu_B) + \kappa_4 f^4(\mu_B) - \kappa_6 f^6(\mu_B) + \dots), \quad (8)$$

where $T_{pc,0} = 156.5(1.5)$ MeV is the crossover temperature at $\mu_B = 0$ and $f(\mu_B) = \mu_B/T$. In recent lattice QCD and other calculations, continuum extrapolated results for the curvature coefficients κ_2 and κ_4 were presented and remarkably agreement was found at least for $\mathcal{O}(\mu_B^2)$: $\kappa_2 = 0.015(1)$ (for the case $\mu_S = 0$) [48–55]. Note that

frequently the crossover line is also parametrized with $f(\mu_B) = \mu_B/T_{pc,0}$ and coefficients $\bar{\kappa}_2, \bar{\kappa}_4$. We can map one parametrization to the other by setting $\bar{\kappa}_2 = \kappa_2$ and $\bar{\kappa}_4 = \kappa_4 - 2\kappa_2\bar{\kappa}_2$, with differences remaining at $\mathcal{O}(\mu_B^6)$. Our CEP location for $N_\tau = 6$ is roughly in agreement with the $\mathcal{O}(\mu_B^2)$ parametrization in $f(\mu_B) = \mu_B/T$. This parametrization is shown in Fig. 1 as dashed line. However, in the region where the CEP is located the contribution of the $\mathcal{O}(\mu_B^4)$ coefficient would already be significant, i.e., the two $\mathcal{O}(\mu_B^2)$ parametrizations with $f(\mu_B) = \mu_B/T$ and $f(\mu_B) = \mu_B/T_{pc,0}$ differ substantially for $\mu_B > 400$ MeV or $T < 140$ MeV. Plugging μ_B^{CEP} or T^{CEP} into the latter, would increase T^{CEP} or μ_B^{CEP} respectively. We note that current cutoff effects that we observe between $N_\tau = 6$ (multipoint Padé) and $N_\tau = 8$ ([4, 4]-Padé) calculations might hint to a continuum result of $(\mu_B^{\text{CEP}}, T^{\text{CEP}})$ that is consistent with $\bar{\kappa}_4 \approx 0$, which is favored by lattice calculations. Current estimates give $\bar{\kappa}_4 \approx 0.001(7)$ (again for $\mu_S = 0$) [48]. The reason why we are not seriously attempting to perform the continuum extrapolation here is that the $N_\tau = 6$ and $N_\tau = 8$ calculations differ by their methodology and might suffer from different systematic effects.

Our estimate for the CEP location compares favorably with a number of other results and constraints. To begin with, it ought to lie outside the estimated convergence region of the Taylor series for $\log Z_{\text{QCD}}$, i.e., it is expected² that $\mu_B/T \gtrsim 2$ [7,56–58]. Moreover, if the CEP exists, it is expected to occur at a lower temperature than the chiral transition temperature [59], which is known to be 132_{-6}^{+3} MeV [19]. Our estimate conforms to both of these expectations. Additionally it is in rough agreement with recent predictions from Dyson-Schwinger equations [53,60], the functional renormalization group [52], black-hole engineering [61], and from neutron-star observations [62]. Similar to our approach, the conformal Padé applied to the same HotQCD data yields a compatible result

²Strictly speaking, this estimate of the convergence radius depends on, e.g., the temperature. Some of these earlier estimates come from coarse lattices. Still, they indicate convergence in the same general regime.

as well [30]. Finally it approximately agrees with a lattice result that follows the width of the chiral crossover as it approaches zero [63].

We have estimated the CEP location under the assumption it belongs to the 3D, $Z(2)$ universality class, a conjecture for all end points of first-order lines. Another possibility would be to treat β and δ as fit parameters. We do not do this, as our goal is the location of the critical point. Adding further parameters would increase uncertainty substantially. That our fits converge well (for example our best fit has $\chi^2/\text{d.o.f.} = 0.043$) can be viewed as further evidence this assumption is reasonable.

Again, an important limitation of the estimates presented here³ is that they are not extrapolated to the continuum limit. For the multipoint Padé, we are limited to $N_\tau = 6$, and the HotQCD data utilize χ_6^B and χ_8^B on $N_\tau = 8$ lattices. At this stage, it appears clear that both datasets are sensitive to a nontrivial singularity structure in μ_B that is consistent with Lee-Yang edge scaling, but in principle our estimates of the location of μ_B^{CEP} are distorted by cutoff effects. Future work includes a controlled estimate using pure imaginary μ_B data at finer lattice spacings.

Summary. Here we present a new strategy for the critical point search at $\mu_B > 0$ by means of first-principle lattice QCD calculations. Based on rational function approximations of the cumulants of the baryon-number fluctuations at imaginary chemical potential we determine singularities in the complex μ_B plane. We extrapolate these singularities using a scaling ansatz motivated by the temperature scaling of the Lee-Yang edge singularity. The rational function approximations are obtained by a multipoint Padé analysis on a sliding interval embedded in $\mu_B/T \in [-i\pi, i\pi]$. For the $N_\tau = 6$ results we find $T^{\text{CEP}} = 102_{-23}^{+11}$ MeV and $\mu_B^{\text{CEP}} = 428_{-74}^{+162}$ MeV,

³And therefore also for Refs. [30] and [63].

based on $\mathcal{O}(10^5)$ different fits. However we expect that cutoff effects will alter μ_B^{CEP} toward larger values. Our estimate is roughly consistent with other estimates in the literature and also with the current determination of the crossover line.

Acknowledgments. This work was supported by the Deutsche Forschungsgemeinschaft (DFG, German Research Foundation) Proj. No. 315477589-TRR 211, by the PUNCH4NFDI consortium supported by the Deutsche Forschungsgemeinschaft (DFG, German Research Foundation) with Project No 460248186 (PUNCH4NFDI) and by INFN (Istituto Nazionale di Fisica Nucleare) under research project *i.s. QCDLAT*. In its early phase this work also received funding from the European Union’s Horizon 2020 research and innovation programme under the Marie Skłodowska-Curie Grant Agreement No. 813942 (*EuroPLEx*). Numerical calculations have been made possible through EuroHPC JU and PRACE grants at CINECA, Italy on Leonardo and Marconi100, and through the Gauss Centre for Supercomputing e.V. ([65]) on the GCS Supercomputer JUWELS [66] at Jülich Supercomputing Centre (JSC). Additional calculations have been performed on Leonardo under the INFN-CINECA agreement for HPC and on the GPU clusters at Bielefeld University, Germany. We also acknowledge support of the Bielefeld NPC.NRW team. D. A. C. was supported by the National Science Foundation under Grant No. PHY20-13064. K. Z. acknowledges support by the project “Nonperturbative aspects of fundamental interactions, in the Standard Model and beyond” funded by MUR, Progetti di Ricerca di Rilevante Interesse Nazionale (PRIN), Bando 2022, Grant No. 2022TJFCYB (CUP I53D23001440006).

Data availability. The data that support the findings of this article are openly available [64], embargo periods may apply.

-
- [1] I. M. Barbour, S. E. Morrison, E. G. Klepfish, J. B. Kogut, and M.-P. Lombardo, *Nucl. Phys. B, Proc. Suppl.* **60**, 220 (1998).
 - [2] Z. Fodor and S. Katz, *Phys. Lett. B* **534**, 87 (2002).
 - [3] P. de Forcrand and O. Philipsen, *Nucl. Phys.* **B642**, 290 (2002).
 - [4] M. D’Elia and M.-P. Lombardo, *Phys. Rev. D* **67**, 014505 (2003).
 - [5] R. V. Gavai and S. Gupta, *Phys. Rev. D* **68**, 034506 (2003).
 - [6] C. R. Allton, M. Doring, S. Ejiri, S. J. Hands, O. Kaczmarek, F. Karsch, E. Laermann, and K. Redlich, *Phys. Rev. D* **71**, 054508 (2005).
 - [7] D. Bollweg, J. Goswami, O. Kaczmarek, F. Karsch, S. Mukherjee, P. Petreczky, C. Schmidt, and P. Scior (HotQCD Collaboration), *Phys. Rev. D* **105**, 074511 (2022).
 - [8] S. Borsanyi, Z. Fodor, J. N. Guenther, S. K. Katz, K. K. Szabo, A. Pasztor, I. Portillo, and C. Ratti, *J. High Energy Phys.* **10** (2018) 205.
 - [9] S. Borsányi, Z. Fodor, J. N. Guenther, R. Kara, S. D. Katz, P. Parotto, A. Pásztor, C. Ratti, and K. K. Szabó, *Phys. Rev. Lett.* **126**, 232001 (2021).
 - [10] S. Mondal, S. Mukherjee, and P. Hegde, *Phys. Rev. Lett.* **128**, 022001 (2022).

- [11] S. Mitra, P. Hegde, and C. Schmidt, *Phys. Rev. D* **106**, 034504 (2022).
- [12] STAR Collaboration, *Phys. Rev. Lett.* **135**, 142301 (2025).
- [13] J. Adam *et al.* (STAR Collaboration), *Phys. Rev. Lett.* **126**, 092301 (2021).
- [14] D. Bollweg, D. A. Clarke, J. Goswami, O. Kaczmarek, F. Karsch, S. Mukherjee, P. Petreczky, C. Schmidt, and S. Sharma (HotQCD Collaboration), *Phys. Rev. D* **108**, 014510 (2023).
- [15] J. Goswami (HotQCD Collaboration), *Proc. Sci. LATTICE2022* (2023) 149 [arXiv:2212.10016].
- [16] P. Dimopoulos, L. Dini, F. Di Renzo, J. Goswami, G. Nicotra, C. Schmidt, S. Singh, K. Zambello, and F. Ziesché, *Phys. Rev. D* **105**, 034513 (2022).
- [17] C.-N. Yang and T. D. Lee, *Phys. Rev.* **87**, 404 (1952).
- [18] M. E. Fisher, *Phys. Rev. Lett.* **40**, 1610 (1978).
- [19] H. T. Ding *et al.* (HotQCD Collaboration), *Phys. Rev. Lett.* **123**, 062002 (2019).
- [20] E. Follana, Q. Mason, C. Davies, K. Hornbostel, G. P. Lepage, J. Shigemitsu, H. Trotter, and K. Wong (HPQCD Collaboration and UKQCD Collaboration), *Phys. Rev. D* **75**, 054502 (2007).
- [21] L. Altenkort, D. Bollweg, D. A. Clarke, O. Kaczmarek, L. Mazur, C. Schmidt, P. Scior, and H.-T. Shu, *Proc. Sci. LATTICE2021* (2022) 196 [arXiv:2111.10354].
- [22] L. Mazur *et al.* (HotQCD Collaboration), *Comput. Phys. Commun.* **300**, 109164 (2024).
- [23] M. A. Clark and A. D. Kennedy, *Phys. Rev. Lett.* **98**, 051601 (2007).
- [24] A. Bazavov *et al.*, *Phys. Rev. D* **85**, 054503 (2012).
- [25] A. Bazavov *et al.* (HotQCD Collaboration), *Phys. Rev. D* **90**, 094503 (2014).
- [26] D. Bollweg, J. Goswami, O. Kaczmarek, F. Karsch, S. Mukherjee, P. Petreczky, C. Schmidt, and P. Scior (HotQCD Collaboration), *Phys. Rev. D* **104**, 074512 (2021).
- [27] S. Singh, M. Cipressi, and F. Di Renzo, *Phys. Rev. D* **109**, 074505 (2024).
- [28] G. Basar, G. V. Dunne, and Z. Yin, *Phys. Rev. D* **105**, 105002 (2022).
- [29] G. Basar, *Phys. Rev. Lett.* **127**, 171603 (2021).
- [30] G. Basar, *Phys. Rev. C* **110**, 015203 (2024).
- [31] D. A. Clarke, K. Zambello, P. Dimopoulos, F. Di Renzo, J. Goswami, G. Nicotra, C. Schmidt, and S. Singh, *Proc. Sci. LATTICE2022* (2023) 164 [arXiv:2301.03952].
- [32] C. Schmidt, D. A. Clarke, P. Dimopoulos, F. Di Renzo, J. Goswami, S. Singh, V. V. Skokov, and K. Zambello, *Proc. Sci. LATTICE2023* (2024) 167 [arXiv:2401.07790].
- [33] J. J. Rehr and N. D. Mermin, *Phys. Rev. A* **8**, 472 (1973).
- [34] C. Nonaka and M. Asakawa, *Phys. Rev. C* **71**, 044904 (2005).
- [35] P. Parotto, M. Bluhm, D. Mroczek, M. Nahrgang, J. Noronha-Hostler, K. Rajagopal, C. Ratti, T. Schäfer, and M. Stephanov, *Phys. Rev. C* **101**, 034901 (2020).
- [36] M. Kahangirwe, S. A. Bass, E. Bratkovskaya, J. Jahan, P. Moreau, P. Parotto, D. Price, C. Ratti, O. Soloveva, and M. Stephanov, *Phys. Rev. D* **109**, 094046 (2024).
- [37] S. El-Showk, M. F. Paulos, D. Poland, S. Rychkov, D. Simmons-Duffin, and A. Vichi, *J. Stat. Phys.* **157**, 869 (2014).
- [38] A. Connelly, G. Johnson, F. Rennecke, and V. Skokov, *Phys. Rev. Lett.* **125**, 191602 (2020).
- [39] F. Rennecke and V. V. Skokov, *Ann. Phys. (Amsterdam)* **444**, 169010 (2022).
- [40] G. Johnson, F. Rennecke, and V. V. Skokov, *Phys. Rev. D* **107**, 116013 (2023).
- [41] F. Karsch, C. Schmidt, and S. Singh, *Phys. Rev. D* **109**, 014508 (2024).
- [42] M. A. Stephanov, *Phys. Rev. D* **73**, 094508 (2006).
- [43] See Supplemental Material at <http://link.aps.org/supplemental/10.1103/y6kg-ry8x> for more detailed information on the sliding window analysis to extract poles from the multipoint Pade approximations to the lattice data, on the statistical analysis of the scaling fits, and the final error analysis.
- [44] L. Altenkort, D. A. Clarke, J. Goswami, and H. Sandmeyer, *Proc. Sci. LATTICE2023* (2023) 136 [arXiv:2308.06652].
- [45] F. Cuteri, J. Goswami, F. Karsch, A. Lahiri, M. Neumann, O. Philipsen, C. Schmidt, and A. Sciarra, *Phys. Rev. D* **106**, 014510 (2022).
- [46] F. Di Renzo, D. A. Clarke, P. Dimopoulos, J. Goswami, C. Schmidt, S. Singh, and K. Zambello, *Proc. Sci. LATTICE2023* (2024) 169 [arXiv:2401.09619].
- [47] M. S. Pradeep and M. Stephanov, *Phys. Rev. D* **100**, 056003 (2019).
- [48] A. Bazavov *et al.* (HotQCD Collaboration), *Phys. Lett. B* **795**, 15 (2019).
- [49] S. Borsanyi, Z. Fodor, J. N. Guenther, R. Kara, S. D. Katz, P. Parotto, A. Pasztor, C. Ratti, and K. K. Szabo, *Phys. Rev. Lett.* **125**, 052001 (2020).
- [50] R. Bellwied, S. Borsanyi, Z. Fodor, J. Günther, S. D. Katz, C. Ratti, and K. K. Szabo, *Phys. Lett. B* **751**, 559 (2015).
- [51] C. Bonati, M. D’Elia, F. Negro, F. Sanfilippo, and K. Zambello, *Phys. Rev. D* **98**, 054510 (2018).
- [52] W.-j. Fu, J. M. Pawłowski, and F. Rennecke, *Phys. Rev. D* **101**, 054032 (2020).
- [53] F. Gao and J. M. Pawłowski, *Phys. Lett. B* **820**, 136584 (2021).
- [54] M. S. Ali, D. Biswas, A. Jaiswal, and H. Mishra, *Phys. Rev. D* **109**, 114017 (2024).
- [55] H. T. Ding, O. Kaczmarek, F. Karsch, P. Petreczky, M. Sarkar, C. Schmidt, and S. Sharma, *Phys. Rev. D* **109**, 114516 (2024).
- [56] M. Giordano and A. Pásztor, *Phys. Rev. D* **99**, 114510 (2019).
- [57] M. Giordano, K. Kapas, S. D. Katz, D. Negradi, and A. Pasztor, *Phys. Rev. D* **101**, 074511 (2020); **104**, 119901(E) (2021).
- [58] S. Mukherjee and V. Skokov, *Phys. Rev. D* **103**, L071501 (2021).
- [59] F. Karsch, *Proc. Sci. CORFU2018* (2019) 163 [arXiv:1905.03936].
- [60] P. J. Gunkel and C. S. Fischer, *Phys. Rev. D* **104**, 054022 (2021).

- [61] M. Hippert, J. Grefa, T. A. Manning, J. Noronha, J. Noronha-Hostler, I. P. Vazquez, C. Ratti, R. Rougemont, and M. Trujillo, *Phys. Rev. D* **110**, 094006 (2024).
- [62] C. Ecker, N. Jokela, and M. Järvinen, [arXiv:2506.10065](https://arxiv.org/abs/2506.10065).
- [63] V. V. Braguta, M. N. Chernodub, A. Y. Kotov, A. V. Molochkov, and A. A. Nikolaev, *Phys. Rev. D* **100**, 114503 (2019).
- [64] F. Di Renzo, D. A. Clarke, P. Dimopoulos, J. Goswami, C. Schmidt, S. Singh, and K. Zambello, [10.4119/unibi/3007759](https://doi.org/10.4119/unibi/3007759) (2025).
- [65] <http://www.gauss-centre.eu>.
- [66] Jülich Supercomputing Centre, *J. Large-Scale Res. Facil.* **7**, A183 (2021).